https://ntrs.nasa.gov/search.jsp?R=19880013459 2020-03-20T06:14:00+00:00Z

13 Salan 1N-90-CR

REPRINTS PERMOULE D 141243 248.

SPECKLE INTERFEROMETRY OF ASTEROIDS NAGW-867 February 1, 1987 – January 31, 1988 FINAL REPORT

Jack Drummond Steward Observatory University of Arizona Tucson, Arizona 85721

May 31, 1988

(NASA-CR-180438) SPECKLE INTERFEROMETRY OF N88-22843 ASTEROIDS Final Report, 1 Feb. 1987 - 31 Jan. 1988 (Arizona Univ.) 24 p CSCL 03B

Unclas G3/90 0141243

Abstract

This final report for NASA Contract NAGW867 consists of abstracts of the first three papers in a series of four appearing in *Icarus* that were funded by the preceding contract NAGW224:

1) Speckle Interferometry of Asteroids I. 433 Eros,

2) Speckle Interferometry of Asteroids II. 532 Herculina,

3) Speckle Interferometry of Asteroids III. 511 Davida and its Photometry; the abstract of the fourth acknowledged to NAGW867:

4) Speckle Interferometry of Asteroids IV. Reconstructed Images of 4 Vesta; and a review (complete copy enclosed) of the results from the asteroid speckle interferometry program at Steward Observatory prepared for the Asteroids II book:

5) Speckle Interferometry of Asteroids.

Two papers on asteroids, indirectly related to speckle interferometry, were written in part under NAGW867. One is in press and its abstract is included:

6) Photometric Geodesy of Main-Belt Asteroids. II. Analysis of Lightcurves for Poles, Periods, and Shapes;

and the other, which has been submitted to Icarus, is included in full:

7) Triaxial Ellipsoid Dimensions and Rotational Pole of 2 Pallas from Two Stellar Occultations.

SPECKLE INTERFEROMETRY OF ASTEROIDS Jack D. Drummond and E. Keith Hege Steward Observatory, University of Arizona

Abstract

Assuming that an asteroid can be treated as a smooth, featureless triaxial ellipsoid rotating about its shortest axis, we summarize Steward Observatory's two dimensional power spectra analysis for speckle interferometry observations of six asteroids. The poles and triaxial ellipsoid dimensions of 4 Vesta, 433 Eros, 511 Davida, and 532 Herculina have been previously reported. New results for 2 Pallas and 29 Amphitrite are given, as well as further results for Vesta. The ultimate goal of image reconstruction has been achieved for Vesta and Eros, and images for these two are displayed. SI and radiometry diameters are compared, and diameters from the two occultations of Pallas are also addressed.

I. INTRODUCTION

Speckle interferometry (SI) is a high angular resolution technique first suggested in the form used here by Labeyrie (1970). To overcome the generally one arcsec limit to resolution imposed by the Earth's atmosphere, and to approach the theoretical resolving power of large telescopes given by the Rayleigh criterion, very short exposures (approximately 0.01 sec) of an object are recorded. These short exposures reveal many small patches of coherence ('apertures'), which can then be combined (Fourier transformed) to obtain information, as in a multiple-aperture interferometer, down to the resolution limit of the telescope. Worden (1979) gives a good description and illustrations of the phenomenon.

Since the angular sizes of all asteroids are less than one arcsec, but many are greater than the theoretical resolution limit of larger telescopes, they are ideal targets for the application of the technique. The Fourier modulus or power spectrum (ps) of the exposures of the 'speckles' contains diffraction limited information of *resolved* asteroids. Although this information can be obtained from either the ps or its transform, the autocorrelation function (ac), it is easier to calibrate observations of extended sources by deconvolving (dividing) with the ps of a point source, which then also removes residual seeing effects as well as the effects of the telescope transfer function. Furthermore, the impact of individual photons can more accurately be gauged in power spectra domain since this photon bias shows up as a simple DC background level in the ps of both the object and the point source, rather than compacted into one or two pixels in the ac domain.

II. AUTOCORRELATION/POWER SPECTRUM ANALYSIS A. Background

For interpretation of the two dimensional autocorrelation (ac) of an asteroid, or its Fourier inverse the two dimensional power spectrum (ps), use is made of what has evolved into a standard set of assumptions for most techniques, SI and photometry in particular. An asteroid is considered to be a smooth (no major topographic features such as craters, mountains, etc.), featureless (no albedo variation over its surface), uniformly bright (geometric scattering; no limb darkening) triaxial ellipsoid (axes diameters $a \ge b \ge c$) rotating about its shortest axis. Under these assumptions the asteroid ellipsoid model will project onto the plane of the Earth's sky a series of ellipses as the body rotates. The observed major and minor axes, and position angle, will vary in a unique fashion as a function of rotation. Drummond et al. (1985a) derive the equations relating these observable parameters back to the triaxial ellipsoid axes dimensions and to the three Euler angles used to then locate the spin axis direction. Thus a non-linear least squares method can be used on two or more ellipses (or their ac or ps), to find an asteroid's true dimensions and pole.

The assumption of an ellipsoidal shape is a mathematically tractable, first order approximation to the actual shape of an asteroid. Since for most purposes any body can be described by its principal axes ratios, the ellipsoid assumption is a very general and useful abstraction. Departures from the ellipsoid (and perhaps other) assumptions are sometimes evident, but generally as secondary effects. The assumption of a triaxial ellipsoid rotating about its shortest axis is rather standard, and would be a natural stable outcome of a body in gravitational and/or hydrostatic equilibrium, such as would be formed by either coalescence or catastrophic collisions which result in so-called rubble piles (Davis et al. 1979; Farinella et al. 1981; Catullo et al. 1984; Zappala et al. 1984). Rotation about the short axis is the most stable configuration, and even precession induced by perturbations and collisions would be expected to be damped out over a small fraction of the lifetime of the Solar System (Burns and Tedesco 1979).

For dark atmosphereless bodies observed at low solar phase angles uniform

brightness is to be expected for all reasonable scattering laws (Dollfus and Zellner 1979). Moreover, limb darkening, which may be 5-10% for completely smooth bodies, is shown to be reduced to less than 5% in meteorites by roughness (French and Veverka 1983). Deformation of a triaxial ellipsoid shape by the presence of mountains, craters, etc., might be important for smaller bodies, but should be negligible for larger asteroids. Even with a random distribution of such deformations, it is still possible to treat the object as a triaxial ellipsoid with noise (irregularities of outline). And unless the deformation has a different albedo, it has no effect on SI measurements until it lies on the limb. Similarly, Fulchignoni and Barucci (1984) have shown that even for the largest craters known (in terms of the body diameter), for Phobos, Mimas, and Thetis, the presence of a crater with the same albedo as the surrounding asteroid material cannot be detected in a lightcurve. (See also the chapter by Magnusson et al. in this book for further justification of the adopted assumptions). Thus we proceed to recount the results of ps analysis of asteroids performed at Steward Observatory with the above assumptions.

B. Results from Power Spectrum Analysis 2 Pallas

In an attempt to use asteroids as calibration objects for SI, 2 Pallas was observed in 1979 (Hege et al. 1980a;1980b) and found to be extremely elongated. The notion of asteroid satellites was in vogue at the time, and these observations were interpreted as indications for a large Pallas satellite. However, this first exploratory effort revealed the necessity for much better calibration of the point spread function, the telescope transfer function, and the geometric distortion introduced by the detector. Furthermore, it was then realized that in order to properly derive the dimensions of an asteroid it needs to be observed throughout its rotation, and in fact such a procedure could lead to a pole determination as well.

On April 9 and 10, 1982, nine observations were made at Steward Observatory's 2.3m telescope with the same equipment as used for the other asteroids since reported in the literature. The results from these Pallas observations are given (for the first time) in Table I. Substantial, systematic departures from a triaxial ellipsoid fit are evident, which we have come to realize as characteristic of the impact of albedo features on our ps analysis.

Pallas is the only asteroid with two well observed stellar occultation outlines,

which are free from albedo effects and which give apparently very reliable direct measurements of its size and shape at two epochs. In considering these occultations, and the two models of the triaxial ellipsoid shape and rotational pole derived from them by Wasserman et al. (1979) and Magnusson (1986), it can be shown that neither model yields the occultation outlines as observed. Drummond and Cocke (1988) show that with the ellipsoid equations at the heart of the SI ps analysis derived in Drummond et al. (1985a), two occultations give a narrowly defined pole (to within a two-fold sense of rotation ambiguity) and triaxial dimensions. Taking the major and minor axes dimensions and the position angle for the two events as given by Wasserman et al. (1979) and as reported by Dunham in a private communication to Magnusson (1986), the c axis is found to be no greater than 120 km. Since this is unrealistically small, and since the first occultation had much larger uncertainties on the measured parameters than the second, a range in solutions is found by varying the first occultation parameters by their uncertainties. It then becomes obvious that the size of the outline on the first occasion was (only slightly) overestimated, since only smaller dimensions yield better (larger c) solutions. Taking the average and standard deviations for the various possible realistic ($c \geq 300$ km) solutions results in a pole at (70; -15) or (250; +15) with a 9° radius error circle, and dimensions of $596(\pm 19)x528(\pm 1)x407(\pm 55)$.

The weighted averages between the direct techniques of SI and occultations are given for the axial dimensions in Table II. Because of the geometries of the observations, SI determines the c axis better than the occultations, but the occultations define the b axis more precisely. Lebofsky et al. (1987) have recently revised the radiometric scale with Ceres and Pallas occultation results and derive an average diameter of 532km for Pallas. The IRAS diameter (Matson *et al.* 1986) is 523 ± 20 . The mean diameter $(abc)^{1/3}$ of the model of Pallas from SI and the occultations given in Table II is 528km, with a range of 504 for the minimum cross section seen at equatorial aspects to 552 for the maximum cross section seen at polar aspects. The pole in Table II is the average between the speckle pole at (100;-22), the occultation pole from the mean of the possible solutions at (70;-15), and the pole at (54;-6) from lightcurve analyses by Magnusson (1986).

4 Vesta

Departing from our traditional intensified photon counting video raster detec-

tor in favor of Harvard's PAPA and Stanford's MAMA two-dimensional photon counting arrays, we have obtained excellent observations of 4 Vesta. As reported by Drummond et al. (1988a), ten observations were made with the PAPA detector over two nights in November, 1983. Triaxial ellipsoid dimensions and the usual two poles were obtained from ps analysis. The superior characteristics and geometric fidelity of the detector allowed successful image reconstructions, discussed further in the next section. Three years later, over three nights in October, 1986, we obtained some 65 observations with the MAMA detector, which fully corroborated the results from the earlier run. In fact the two-fold ambiguity inherent to SI, which leads to a two-fold ambiguity in the location of the rotational pole and is normally resolved by appealing to lightcurves, is fully resolved with SI alone because of the differing geometries for the two runs. The two possible poles from the PAPA run were (336;+55) and (209;-50), while the two from the MAMA run were around (324;+52) and (83;-64); the correct region of the pole is obvious. Treating the results from each of the three nights of the MAMA run independently, the weighted average of four pole determinations involving 10,17,23, and 25 observations from the two runs is given in Table I, and since it can be regarded as definitive, is repeated in Table II.

In a similar fashion, the weighted average of the four SI triaxial ellipsoid dimension determinations are given in both Tables I and II. The mean diameter of Vesta would vary between extremes of 498 and 549 km, with $(abc)^{1/3} = 520$. This is much closer to the radiometrically determined 530 in the TRIAD file than the 579 from polarimetry. (Note that these diameters were inadvertently attributed to the opposite techniques by Drummond et al. 1988a). Brown et al. (1982) have suggested that the radiometric diameters in the TRIAD file should be reduced by 5% on the average, which would make Vesta's radiometric diameter 504km. The IRAS diameter is listed as 501 ± 24 . It appears that most of the radiometric observations were made near Vesta's equatorial plane, where the average diameter would range between 498 and 514 km.

29 Amphitrite

Previously unpublished results from ps analysis of five observations of Amphitrite on July 1, 1985, are given in Table I. It is well known from its irregular photoelectric lightcurves that Amphitrite must possess substantial albedo variations over its surface, making conclusions and interpretations somewhat dangerous. Nevertheless, with the large number of lightcurves available and the converging consensus of axial ratios from photometric analysis, this asteroid is suggested as a calibration standard for S asteroids in the chapter on poles and shapes by Magnusson et al. in this book.

From the photometric determinations of the rotational axis listed in Part VI of this book, two ambiguous poles emerge, at (139;-33) and (328;-41), both with about 15° errors. Considering the two possible poles from SI listed in Table I, the pole ambiguity is resolved in favor of the first listed pole; the average from the six photometric and one SI determination is listed in Table II.

The consensus axial ratios for Amphitrite given in the chapter by Magnusson et al. includes the ratios of $a/b = 1.22 \pm .17$ and $b/c = 1.06 \pm .13$ contributed by SI. In light of the good agreement between the photometric and SI axial ratios, it is somewhat surprising to find that the mean TRIAD polarimetric and radiometric diameters of 197 and 200km, respectively, and the IRAS value of 219 ± 5 do not agree that well with the mean SI diameter of 160, with an extreme range of 148 to 168 corresponding to $(bc)^{1/2}$ and $(ab)^{1/2}$, respectively. The reason for the discrepancy undoubtedly lies in the surface albedo structure inferred from the lightcurves, but it is not clear whether this influences SI or radiometry more. Adjusting the mean diameter to 190km, midway between the SI and the IRAS values, and adopting the consensus axial ratios of 1.21x1.08x1.00, the best estimate of the dimensions are given in Table II, where the uncertainties are the vector sum of the uncertainties in Table I and the differences between the dimensions in the two tables.

433 Eros

Key to the development of the present form of speckle interferometry is the small Earth-approaching asteroid Eros. Spurred by observations separated by a month, but for substantially different geometries at high solar phase angles, equations expressing the projection of triaxial ellipsoids to ellipses were derived and converted into a non-linear method to relate the observed major and minor axes and position angles back to the triaxial ellipsoid dimensions and rotational pole (Drummond et al. 1985a). Figure 1 shows the seven 2-D power spectra from two nights in December 1981, arranged in order of rotational phase. The lower half of each frame is the actual power spectra, and the upper half is the ellipse fit to the ps. Since ps are mirror symmetric, it is sufficient to fit and display a half-plane. If Eros were a smooth trixial ellipsoid these elliptical power spectra would have the same shape as the ellipses projected onto the plane of the sky. At the very least, Fig. 1 clearly shows an elongated object spinning in space when the sub-Earth point was close to the rotational pole.

The results from the two runs are summarized in Table I. The pole is resolved from SI alone because of the differing geometries of the two runs, and is consistent with the same resolution known from photometric methods. Table II gives the average of the eight most recent pole determinations (including the SI pole) listed in Part VI of this book. The dimensions in Table II are the averages and standard deviations from SI, radiometry (Lebofsky and Reike 1979), radar (Jurgens and Goldstein 1976), and the consensus model of Zellner (1976), all listed by Drummond et al. (1985a). The biggest discrepancy between the SI and other results appears to be in the pole, but given the small target, the large (40 and 52°) solar phase angles involved in the SI observations and the distinctly non-ellipsoid shape shown in the reconstructed image in the next section, the agreement is actually quite good.

511 Davida

From only five observations on one night covering only a quarter of a rotation, the results given in Table I were derived from ps analysis (Drummond et al. 1986). Although it was suggested that the difficulty in finding a triaxial ellipsoid solution was perhaps due to albedo features, subsequent photometric analysis strongly suggests the contrary, that Davida is very smooth and uniform. In fact, Magnusson et al in this book offer it as the best calibration standard available. Despite the large error associated with the SI poles, it is still easy to resolve the ambiguity in photometric pole determinations. Part VI in this book shows that the two possible poles are located around (95;+30) and (300;+35), but considering the two possible poles from SI in Table I it is easy to identify the correct one.

Because of the small number of observations the SI diameters have large associated errors. Therefore, it is not surprising that the mean SI diameter of 350km, with a range of $(bc)^{1/2} = 304$ to $(ab)^{1/2} = 408$, is larger than the TRIAD radiometric diameter of 323km or the downward revised 307km, or the IRAS diameter of 337 ± 5 . For our best estimate of the diameters in Table II we use the well determined axial ratios from the Magnusson et al. chapter and a mean diameter midway between the IRAS and SI values. The preferred uncertainties are then simply the difference between the diameters in Tables I and II. The errors from SI are not used because they are unrealistic. The diameters used in Table II are certainly within the quoted uncertainties of the true values without considering the SI errors.

532 Herculina

Herculina presents a peculiar case. Its sometimes single max/min and sometimes double max/min lightcurves have proven difficult to explain. The first attempt to develop a model was given by Drummond et al. (1985b) to explain the SI observations. The pole and dimensions from ps analysis are given in Table I. In order to account for peculiar SI measurements at certain rotational phases, and to account for the lightcurve history, a bright spot was postulated. However, with a photometric astrometry method, Taylor et al. (1987) found an entirely different pole, and offered a spherical model with two dark spots. But this model was in turn rejected because Lebofsky et al. (1988) showed from thermal lightcurves that the visible lightcurve amplitude was caused by changing cross sectional area and therefore Herculina could not be a sphere. Current efforts (Drummond et al. 1988b) are concentrating on a triaxial ellipsoid model with major albedo or topographic (crater) features.

It would be premature to list parameters with any degree of confidence in Table II. While the original TRIAD radiometric diameter of 220km is in good agreement with the SI mean diameter of 231km, the revised diameter of 209 falls outside the range inferred from SI of 216 to 239km. However, the IRAS diameter of 231 ± 4 agrees exactly with the SI mean diameter. Further observations with all techniques are needed before anything firm can be said about the shape of Herculina, but its average size seems well-determined and the pole from Taylor *et al.* (1987) at (96;-1) derived from the timings of lightcurve features appears firm.

Comparison of SI to other Diameters

Fig. 2 shows the mean diameters $(abc)^{1/3}$ from Table I plotted against the radiometric diameters from the IRAS file (Matson *et al.* 1986). The vertical lines on the mean diameters are not error bars, but represent the extreme possible range of cross section, from $(bc)^{1/2}$ in the equatorial plane to $(ab)^{1/2}$ at polar aspects according to the SI values in Table I. Observations should statistically tend to occur near the bottom of this range since an asteroid's orbit guarantees that the

Earth will cross the equatorial plane every sidereal period, but only in exceptional circumstances (the rotational pole lying in the orbital plane) could a polar view be provided. The horizontal lines are error bars from the IRAS list. For comparison, the diameters from the TRIAD file (Morrison and Zellner 1979), reduced by the 5% suggested by Brown *et al.* (1982), are shown as open circles. The Pallas diameter, however, is from Lebofsky et al. (1986), where a refined thermal model was used. Also note that Eros does not have an IRAS measurement, so only a reduced TRIAD diameter is used.

Except for 29 Amphitrite, the agreement between the SI and radiometric diameters is quite good. Pallas' radiometric diameter has been considerably reduced from the original TRIAD diameter of 589 km. For two asteroids (511 and 532) the agreement between the SI and IRAS diameters are much better (moved to the right in Fig. 2) than the TRIAD diameters with the indiscriminate 5% reduction. Perhaps some of the discrepancies in Fig. 2 can be explained by albedo features since such features can have an impact on diameters derived from SI ps analysis, and could move the SI diameters up or down in the figure. Or perhaps individual treatment of asteroids with non-standard thermal modeling would reduce the discrepancies. One of the strong points about the SI results is that all three axes diameters are derived at once, so that the vertical lines can be drawn in the first place. With SI each asteroid is treated independently and completely, requiring no assumptions or modelling with indeterminant parameters.

III. IMAGE RECONSTRUCTION A. Background

The image of an object, $O(\mathbf{r})$, can be reconstructed from measurements of the object's complex visibility function by inverse Fourier transform:

 $O(\mathbf{r}) = FT^{-1}(V(\mathbf{f}))$, where **r** and **f** represent image ordinary space (x,y) and image frequency space (u,v), respectively. The complex visibility $V(\mathbf{f})$, measured in image frequency space, is conveniently represented, after Euler, in terms of its amplitude and phases: $V(\mathbf{f}) = A(\mathbf{f})e^{i\phi(\mathbf{f})}$. The image amplitudes $A(\mathbf{f})$ are just the square root of the image power spectra calibrated as required for the ps/ac analysis as described above.

The image phase measurements in the Knox-Thompson approximation are obtained from the same complex Fourier transform, $I_k(\mathbf{f}) = FT(\mathbf{i}_k(\mathbf{r}))$ of the observed specklegrams $i_k(\mathbf{r})$. The ps is accumulated as the time averaged square modulus of the set k = 1, 2, 3, ..., m, of Fourier transformed specklegrams,

 $PS(\mathbf{f}) = \langle I_k^*(\mathbf{f}) I_k(\mathbf{f}) \rangle_m$ where $\langle \dots \rangle_m$ denotes the average. Knox and Thompson (1974) showed that phase differences, and hence by numerical integration the phases, can be accumulated from two quite similar complex accumulations in the two dimensional $\mathbf{f} = (u, v)$ plane:

 $CS_u(\mathbf{f}) = \langle I_k^*(u,v)I(u+1,v) \rangle_m$ and $CS_v(\mathbf{f}) = \langle I_k^*(u,v)I(u,v+1) \rangle_m$.

Just as there is an image plane analog of the ps (the ac), there are equivalently image plane analogs to the two phase difference cross spectra, the two corresponding complex cross correlation functions. Hence the complex visibility measurements can be made in either data domain. The phases and amplitudes can be combined to retrieve the image of the object (see Drummond et al., 1988, for details of the procedures as applied to Vesta).

B. Images of 433 Eros and 4 Vesta

In collaboration with the speckle group at Steward Observatory, R. H. Bates of the University of Canterbury in New Zealand has produced a reconstructed image of the second observation of Eros on December 18, 1981, which corresponds to the third ps from the right in the top row in Fig. 1. (In Drummond et al. 1985a, the observation is the sixth point in Figs. 2 and 3, the third frame in Fig. 9, and is the sixth drawing in Fig. 10.) Line drawings of this projected image are given in Fig. 3a, and intensity profiles are presented in two different perspectives in 3b and 3c. (The intensities between the dotted and solid line in the projected image and exterior to the dotted line in the intermediate perspective are rather uncertain because of instrumental artifacts along these rasters.) The solar phase angle at the time was 40° and the latitude of the sub-Earth point was -74° according to the pole in Table I, or -62° with the pole from Table II. The projected image reveals that Eros is shaped more like a peanut than a strict triaxial ellipsoid and the intensity profiles suggest that the brightness distribution across the small asteroid is not uniform at 40° solar phase angles, both of which would contribute to the difference between the poles in the two tables. Does this picture of Eros correspond to the idea that it may be a 'chip' off a larger body or does it look more like the nucleus of a comet?

Eight images of Vesta were reconstructed and discussed by Drummond et al. (1988a). The data were taken with Harvard's PAPA detector, and with the close cooperation of C. Papalilios, P. Nisenson, and S. Ebstein. The images are due to A. Eckart. Although there was a problem with multiple detection of photons, which have since been corrected, the images were sufficient to reveal dark and bright areas on the surface. A spot model was developed based on the images which when combined with the triaxial ellipsoid shape derived from the ps analysis could reproduce all low solar phase angle lightcurves ever taken, down to the rotational phase and amplitude.

From theoretical considerations of its inferred basaltic crust, it could be argued that the derived triaxial shape (Drummond et al. 1988a), where $a/b = 1.10 \pm .04$ from ten observations, cannot be correct, that a/b must be 1.0, and that Vesta is an equilibrium figure (Cellino et al. 1987). It should be pointed out that the SI results are observational, with the model being driven by the images, and not vice versa. However, as the observations stand, the possibility certainly exists that Vesta's a/bratio may be closer to unity, with the observed spots dominating the lightcurves more than the unequal axes. In fact, with some 65 later observations with Stanford's MAMA detector, provided through the courtesy of J. Morgan and J. G. Timothy, the a/b ratio is now considered to be $1.06\pm.04$, as reported in Table I. The question then becomes how close to unity must the ratio be to satisfy theoretical objections. Perhaps analysis of images reconstructed from the newer data set will settle the issue. One from the set of 65 images currently being constructed is shown in Fig. 4.

Acknowledgments

٠.

The results presented in this chapter were obtained under NASA grants NAGW-224 and NAGW-867. The chapter was written with funds from the latter.

References

- Brown, R. H.; Morrison, D.; Telesco, C. M.; and Brunk, W. 1982. Calibration of the radiometric asteroid scale using occultaion diameters. *Icarus* 52: 188-195.
- Burns, J. A., and Tedesco, E. F. 1979. Asteroid lightcurves: Results for rotations and shapes. In Asteroids ed. T. Gehrels, pp. 494-527.: .
- Catullo, V.;Zappala, V.;Farinella, P.;and Paolicchi, P. 1984. Analysis of the shape distribution of asteroids. Astron. and Astrophys. 138: 464-468.
- Cellino, A.;Zappala, V.; DiMartino, M.;and Paolicchi, P. 1987. Flattening, pole and albedo features of 4 Vesta from photometric data. *Icarus* 70: 546-565.
- Davis, D. R.; Chapman, C. R.; Greenberg, R.; and Weidenschilling, S. J. 1979. Collisional evolution of asteroids: Populations, rotations, and velocities. In Asteroids ed. T. Gehrels, pp. 528-557.: .
- Dollfus, A., and Zellner, B. 1979. Optical polarimetry of asteroids and laboratory samples. In Asteroids ed. T. Gehrels, pp. 170-183.: .
- Drummond, J. D., and Cocke, W. J. 1988. Triaxial ellipsoid dimensions and rotational pole of 2 Pallas from two stellar occultations. Subm. to Icarus:
- Drummond, J. D., and Hege, E. K. 1986. Speckle interferometry of asteroids. III. 511 Davida and its photometry. *Icarus* 67: 251-263.
- Drummond, J. D.; Cocke, W. J.; Hege, E. K.; Strittmatter, P. A.; and Lambert, J. V. 1985a. Speckle interferometry of asteroids. I. 433 Eros. *Icarus* 61: 132-151.
- Drummond, J. D.;Hege, E. K.;Cocke, W. J.;Freeman, J. D.;Christou, J. C.; and Binzel, R. P. 1985b. Speckle interferometry of asteroids. II. 532 Herculina. *Icarus* 61: 232-240.
- Drummond, J. D.; Eckart, A.; and Hege, E. K. 1988a. Speckle interferometry of asteroids IV. Reconstructed images of 4 Vesta. *Icarus* 73: 1-14.
- Drummond, J.;Taylor, R.;Greenberg, R.; and Lebofsky, L. 1988b. The mysterious case of 532 Herculina. Paper presented at the Asteroids II conference, March 8-11, 1988: .
- Farinella, P.; Paolicchi, P.; Tedesco, E. F.; and V. Zappala 1981. Triaxial equilibrium ellipsoids among the asteroids?. *Icarus* 46: 113-123.

- French, L. M., and Veverka, J. 1983. Limb darkening of meteorites and asteroids. *Icarus* 54: 38-47.
- Fulchignoni, M., and Barucci, M. A. 1984. The effect of the large crater on the asteroid's lightcurve (Abstract). B.A.A.S. 16: 699.
- Hege, E. K.;Cocke, W. J.;Hubbard, E.;Gesham, M.;Strittmatter, P. A.;Radick, R.;and Worden, S. P. 1980a. Speckle interferometric observations of 2 Pallas (Abstract). B.A.A.S. 12: 509.
- Hege, E. K.;Cocke, W. J.;Hubbard, E. N.;Christou, J.;and Radick, R. 1980b. Possible secondaries of asteroids found by speckle interferometry (Abstract).
 B.A.A.S. 12: 662.
- Jurgens, R. F., and Goldstein, R. M. 1976. Radar observations at 3.5 and 12.5 cm wavelength of asteroid 433 Eros. *Icarus* 28: 1-15.
- Knox, K. T., and Thompson, B. J. 1974. Recovery of images from atmospherically degraded short exposure photographs.. *Astrophys. J.* 193: L45-L48.
- Labeyrie, A. 1970. Attainment of diffraction limited resolution in large telescopes by Fourier analyzing speckle patterns in star images. Astron. and Astrophys. 6: 85-87.
- Lebofsky, L. A., and Reike, G. H. 1979. Thermal properties of 433 Eros. Icarus 40: 297-308.
- Lebofsky, L. A.;Sykes, M. V.;Tedesco, E. F.;Veeder, G. J.;Matson, D. L.;Brown, R. H.;Gradie, J. C.;Feierberg, M. A.;and Rudy, R. J. 1987. A refined 'standard' thermal model for asteroids based on observations of 1 Ceres and 2 Pallas. *Icarus* 68: 239-251.
- Lebofsky, L. A.;Greenberg, R.;Tedesco, E. F.;and Veeder, G. J. 1988. Infrared lightcurvews of asteroids 532 Herculina and 45 Eugenia: Proof of the absence of significant albedo markings. *Icarus* accepted for publication: .
- Magnusson, P. 1986. Distribution of spin axes and senses of rotation for 20 large asteroids. *Icarus* 68: 1-39.
- Morrison, D., and Zellner, B. 1979. Polarimetry and radiometry of the asteroids. In Asteroids ed. T. Gehrels, pp. 1090-1097.: .
- Taylor, R. C; Birch, P. V.;Drummond, J.;Pospieszalska-Surdej, A.; and Surdej, J. 1987. Asteroid 532 Herculina: Lightcurves, pole orientation, and a model. *Icarus* 69: 354-369.

- Wasserman, L. H.;Millis, R. L.;Franz, O. G.;Bowell, E.;White, N. M.;Giclas, H. L.;Martin, L. J.;Elliott, J. L.;Dunham, E.;Mink, D.;Baron, R.;Honeycutt, R. K.;Hendon, A. A.;Kephart, J. E.;A'Hearn, M. F.; Reitsema, H. J.;Radic, R.;and Taylor, G. E. 1979. The diameter of Pallas from its occultation of SAO 85009. Astron. J. 84: 259-268.
- Worden, S. P. 1979. Interferometric determinations of asteroid diameters. In Asteroids ed. T. Gehrels, pp. 119-131.: .
- Zappala, V.;Farinella, P.;Knezevic,Z.;and Paolicchi, P. 1984. Collisional origin of the asteroid families: Mass and velocity distributions. *Icarus* 59: 261-285.

Zellner, B. 1976. Physical properties of asteroid 433 Eros. Icarus 28: 149-153.

Figure Captions

Fig. 1. Two dimensional power spectra of 433 Eros from December 17,18 1981. The first figure contains rings, in outward order, of .3, .1, and .06 arcsec in power spectra domain used for scaling illustrations. The upper part of each frame is the elliptical fit to the lower half.

Fig. 2. SI vs IRAS radiometric diameters. The range in SI diameters, from $(bc)^{1/2}$ to $(ab)^{1/2}$, corresponds to the minimum and maximum possible values according to Table I. The dots and their horizontal error bars are from the IRAS file (Matson *et al.* 1986), and the open circles are TRIAD diameters reduced by 5%, except for 2 Pallas which comes from Lebofsky *et al.* (1987).

Fig. 3. Intensity profiles from a reconstructed image of 433 Eros. 3a is the outline of the asteroid's reconstructed image, 3b and 3c are intensity profiles from different perspectives.

Fig. 4. Reconstructed image of 4 Vesta. To be provided.

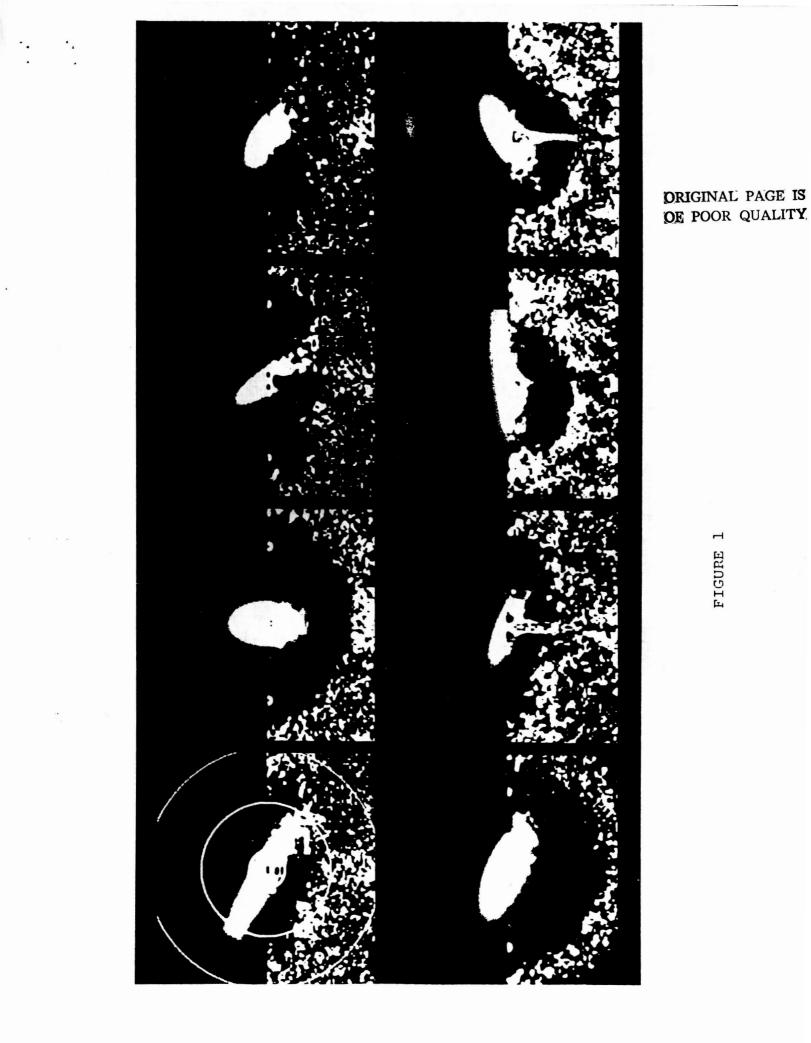
Asteroid	a	Ь	C	Ecliptic Pole (1950
2 Pallas	537 ± 29	488 ± 11	485 ± 11	$100 - 22 \pm 8$
				$295 + 16 \pm 8$
4 Vesta	566 ± 15	532 ± 15	466 ± 15	$327 + 55 \pm 4$
29 Amphitrite	186 ± 18	152 ± 15	144 ± 10	$134 - 36 \pm 12$
				$303 + 35 \pm 12$
433 Eros	41 ± 3	15 ± 2	14 ± 2	$23 + 37 \pm 14$
511 Davida	465 ± 90	358 ± 58	258 ± 356	$196 - 12 \pm 29$
				$291 + 37 \pm 29$
532 Herculina	263 ± 14	218 ± 12	215 ± 12	$132 - 59 \pm 7$
				128 +74 ± 7

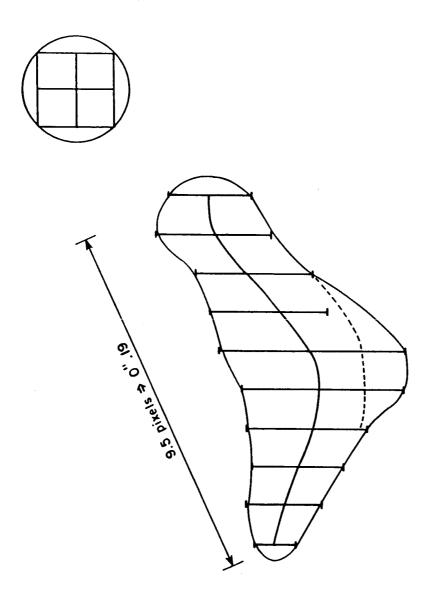
Table I						
Diameters	and	Poles	from	SI		

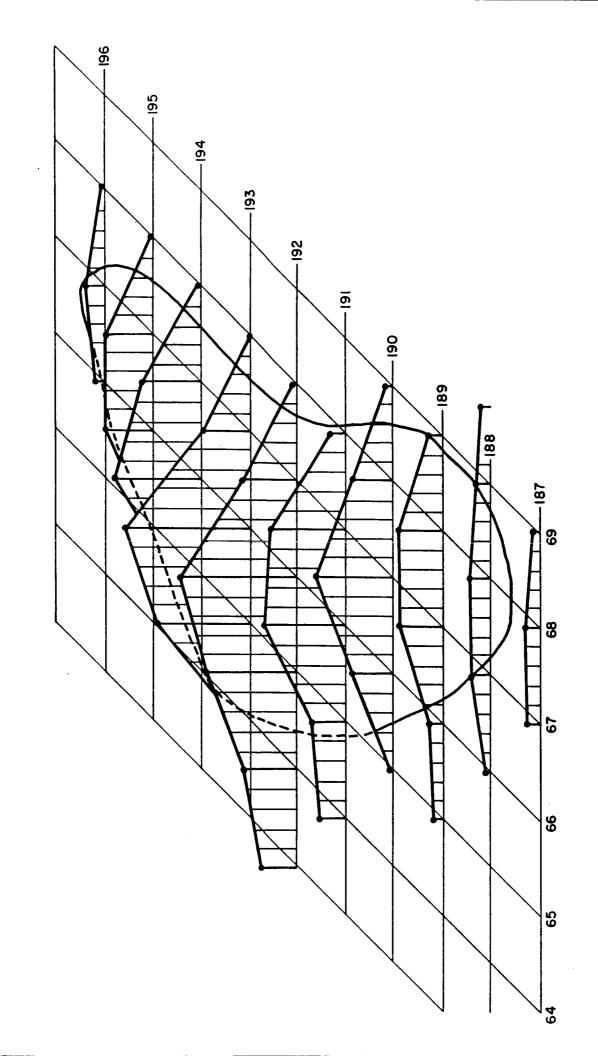
· · · ,

Table IIDiameters and Poles from Combining SI and Others

		-	····		
Asteroid	a	Ь	C	Ecliptic Pole (1950)	
2 Pallas	578 ± 27	528 ± 4	482 ± 15	$74 - 15 \pm 24$	
4 Vesta	566 ± 15	532 ± 15	466 ± 15	$327 + 55 \pm 4$	
29 Amphitrite	210 ± 30	188 ± 39	174 ± 19	$138 - 33 \pm 16$	
433 Eros	38 ± 2	15 ± 1	14 ± 1	$17 + 16 \pm 11$	
511 Davida	417 ± 48	333 ± 25	292 ± 34	$299 + 34 \pm 9$	
532 Herculina	? ± ?	? ± ?	? ± ?	? ± ?	

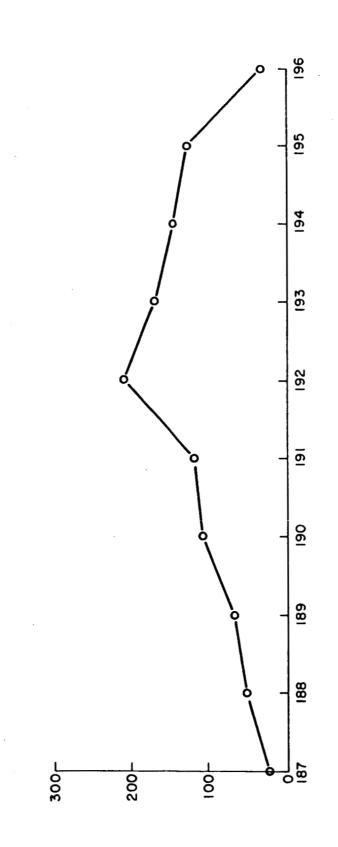


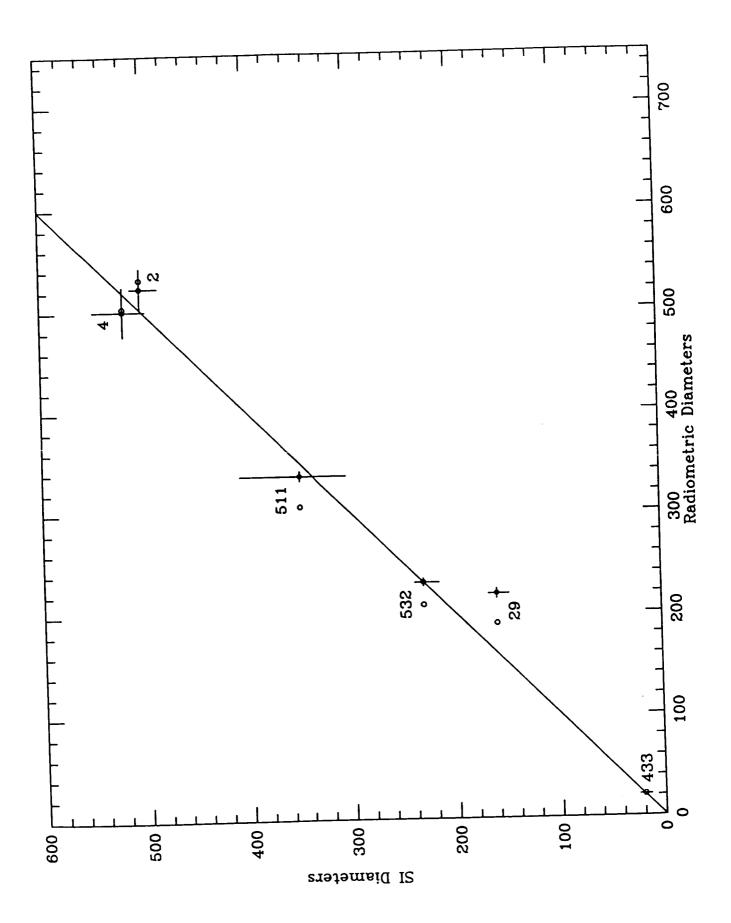




•••

.





· · · · ·